High-frequency vibration of a conformal antenna structure

X Chen[1], **Y Tang**[1], **L Liu**[1], **M Zhao**[1], **V K Punyamurtula**[2], **J Chen**[2], **A Han**[2], and **Y Qiao**[2*]

[1]Department of Civil Engineering and Engineering Mechanics, Columbia University, New York, NY, USA

[2]Department of Structural Engineering, University of California at San Diego, La Jolla, California, USA

The manuscript was received on 2 August 2007 and was accepted after revision for publication on 14 February 2008.

DOI: 10.1243/09544100JAERO268

Abstract: When the functionalities of an antenna and a load-carrying airframe are integrated into a unified structure in an unmanned aerial vehicle, they would affect each other as additional mechanical loading is caused by electromagnetic field. For a low-frequency structural motion, this coupling effect is negligible; for high-frequency vibrations, non-uniform frequency shifts and magnitude variations are predicted.

Keywords: antenna, wing, high-frequency vibration, integrated

1 INTRODUCTION

One of the efficient ways to collect real-time data for both scientific research and military operations is to use small-sized unmanned aerial vehicles (UAVs), which has been an active development area in the past few decades [**1**]. As a UAV operates at a low-altitude level, it can take photos or videos using controlled cameras, analyse air and pollution via remote sensor clusters, and, very often most importantly, monitor local wireless signals through a set of on-board antennas [**2**].

Currently, in many UAVs, antenna systems and airframes are designed separately. According to the bandwidth and nature of communication, the electronic engineer team designs the receiver, amplifier, conditioner, and power supply. Then, the structural engineer team designs the airframe, taking into account the additional drag force and the extra stability requirement. Because of the aerodynamic issues involved, in an ordinary UAV, the antenna should be as small as possible, so that the aircraft can survive adverse operation conditions without losing speed and lift [**3**].

Although this system works quite well for high-bandwidth communications, it fails to meet the functional requirements for low-bandwidth wireless signals such as that of cellular phones, televisions, satellite radios, and so on. According to the basic antenna design theory [**4**], $d = \alpha \cdot B^{-1}$, where d is the antenna size, B the bandwidth, and α a parameter determined by the required gain, material's impedance, antenna shape, and the environmental factors, the details of which are beyond the scope of this study. If the signal frequency is >400 MHz, the required antenna size is usually <0.5 m, which can be relatively well handled by the current aircraft technology. If the signal frequency is <30 MHz, however, the antenna must be >4–5 m. For a small-sized UAV, typically, the length is in the range of 2–3 m and the cross-sectional size of the body is only 0.2–0.6 m. If the antenna system is installed as an attachment to the airframe, it would result in a large, unbalanced drag force. Moreover, the large-sized antenna can make it prohibitively difficult to control the aircraft motion.

Over the years, a number of techniques have been investigated to solve this problem. For instance, by using an array of small antennas, the lower bound of the bandwidth can be compared with that of a single large antenna [**5, 6**]. However, this technique imposes tight constraints on the direction of the flight and the compatibility with environment and therefore is only relevant to some special applications. Additionally, the small antenna components need to be distributed somewhat 'irregularly' in a large area, which still affects the flight operation.

Corresponding author: Department of Structural Engineering, University of California at San Diego, 9500 Gilman Dr MC 0085, La Jolla, CA 92093-0085, USA. email: yqiao@ucsd.edu

Recently, an innovative concept, integrating communication and load-bearing functionalities in a unified structure, has drawn increasing attention [**7–9**], i.e. as appropriate materials, e.g. electroconductive, lightweight, and high-strength composites, are used, the entire framework of UAV can be employed as a conformal antenna. In other words, if the shape of a large antenna can be designed in a way such that its aerodynamic characteristics are acceptable, the problems of flight control and low-bandwidth communication can be solved simultaneously.

One of the concerns for the integrated antenna–airframe (IAA) system is that, as the wireless signals are received, currents could be generated inside the structure. When the aircraft flies across an electromagnetic field, not only the receiver function can be influenced, but also an additional external loading will act on the airframe. For low-frequency mechanical motions, this effect should be negligible, because its magnitude, as will be discussed shortly, is small and over the characteristic time, it can be averaged out. For high-frequency mechanical motions, e.g. vibration modes with frequencies >30 MHz, however, the structural behaviours can be different, which in turn would affect the reception efficiency, as the signal frequency is also in this range. For instance, it has been well known that high-frequency motion of an antenna may cause significant noises [**10**, **11**], which demands high-performance signal-conditioning components and algorithms.

In the current study, through a computer simulation, the change in the vibration mode and frequency in the high-frequency range of a representative IAA structure, which is taken as a free-standing aircraft wing, is investigated; that is, it is assumed that the wings can be employed as an antenna, and therefore the tip-to-tip distance, which is the largest span in a UAV, can be fully used and the bandwidth boundary can be minimized. Owing to the random nature of wireless signals and flight operations, additional loading is analysed along out-of-plane (normal to the wing surface), transverse (within the wing surface and normal to the axial direction), and axial (within the wing surface and parallel to the axial direction) directions. This study also provides useful information for the development of next-generation morphing aircrafts, where a large number of distributed sensors and actuation units will be embedded in the airframes.

2 FINITE-ELEMENT ANALYSIS OF HIGH-FREQUENCY VIBRATION

In the current simulation, the length of the wing is set as 4 m. A schematic of the wing is shown in Fig. 1. The shape is tapered such that on the clamped end (where the wing attaches to a rigid mainframe) the

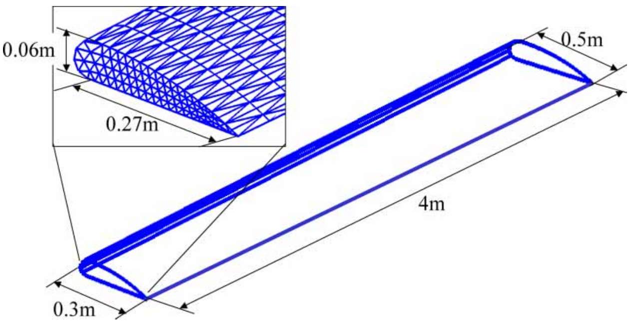

Fig. 1 Geometry of the wing under investigation and a zoom-in view of the finite-element mesh near the free end

width is 0.5 m and the width at the free end is 0.3 m; the tapering function is linear. The top surface of the wing is parabolic, whereas the bottom surface is flat; both ends of the wing are 'sealed' to form a closed structure. The wing is made by a thin aluminium shell with a uniform thickness of 0.01 m. The Young's modulus is 70 GPa, the Poisson's ratio is 0.35, and the weight density is 2.7 Mg/m^3. Although the material and the geometry of the UAV wings may vary in a wide range, the current model should be able to capture the basic mechanisms.

According to the Maxwell equation, as a conductive part moves in an electromagnetic field, a force normal to the moving direction would be generated. In a transient field, the magnitude and direction of the force should vary even if the motion is constant. Consider a beam with an annular cross-section (with very small thickness) under axial load; the frequency shift is of the order of $\varepsilon/10\sqrt{E/4\rho R^2}$, where ε is the axial strain, E the Young's modulus, ρ the density, and R the radius of the beam. When the axial load is of the same order of gravity, one can estimate that for the lowest vibration mode, the frequency shift is at the level of 10^{-3} Hz. For the antenna wing with geometry shown in Fig. 1, in the low-frequency range, it is confirmed that the frequency shifts caused by the additional loadings are negligible – for example, for the frequencies <5 MHz, no shift >1 Hz was observed for the range of load considered. Therefore, the following discussion will be focused on higher-order vibration modes, i.e. those >30 MHz. In this range, because the characteristic time of vibration is much smaller than that of the variation in the external load, it is assumed that the loading is constant during a full cycle. Note that in this model the distribution of the electromagnetic force is uniform.

The simulation was performed using ABAQUS. The finite-element mesh consists of 2400 nodes and 4800 three-node triangular shell elements with reduced integration (S3R). A zoom-in view of the mesh near the free end of the wing is shown in the insert of Fig. 1.

As a first-order approximation, the external loading is set to 1 per cent gravity. Loadings equivalent to 10 and 100 per cent gravity are also analysed, in out-of-plane, transverse, and axial directions. The lower end of the analysed loading range is close to the order of magnitude of the external force on a UAV. For instance, the gravity force of a section of a lightweight conductive composite with the size of $1\,\mu m \times 1\,\mu m \times 0.1$ m is $\sim 10^{-9}$ N [**12**], which is 100 times larger than the electromagnetic force if the current is 10^{-4} mA and the field strength is 10^{-7} T [**13**]. The higher end is discussed for comparison purpose.

3 RESULTS AND DISCUSSION

Figure 2 shows the frequency shifts of the natural (eigen) vibration modes with frequencies >30 MHz when the external loading is normal to the wing surface and pointing downwards. It is remarkable that the frequency shift is highly non-uniform. As the load is equivalent to 1 per cent gravity, most of the high-frequency vibration modes are not affected. Before and after the external loading is applied, the frequency changes of these modes are <1 Hz, within the simulation resolution. However, for a number of isolated vibration modes (the 23rd, 119th, 147th, 151st, 170th, 206th, 290th, 294th, 331st, 355th, 363rd, 379th, 384th, 437th, and 446th modes), the frequency shifts are much larger. For example, the frequency of the 355th mode increases by 4 Hz as the external loading is applied.

As the external loading increases, both the number of affected modes and the magnitude of the frequency shift increase. As the load is equivalent to 10 per cent gravity, the maximum frequency shift, −20 Hz, occurs at the 413th mode, followed by the shift of −16 Hz at the 355th mode. When the load is further increased to 100 per cent gravity, the maximum frequency shift is −196 Hz at the 413th mode, taking place at the initial frequency of ∼51 MHz; the second largest shift is −156 Hz at the 355th mode, whose initial frequency is ∼45 MHz. Clearly, as the external load becomes larger, more work is done during vibration, which, in turn, affects the system potential energy. The kinetic vibration energy, K, can be related to the characteristic frequency through $K = \rho\beta\gamma^2$ [**14**], where β is a system parameter, ρ the density, and γ the frequency. For the lowest natural vibration frequency of a beam, the frequency shift would be nearly proportional to the small strain induced by the external load. In the current situation, however, owing to the shell-like wing geometry, for different high-frequency eigenmodes, the frequency (eigenvalue) may either increase or decrease, indicating that the total vibration energy not only becomes different, but also re-distributes over the frequency domain (i.e. the eigenmode function characterizing the vibration shape is changed), that is, an important factor governing the magnitude and the sign of the frequency shift as well as the eigenmode function is the magnitude of external loading. It can be seen that as the load increases from 1 to 10 per cent gravity, those eigenmodes that have finite frequency shifts, $\Delta\gamma$, at the smaller load retain the frequency shift characteristic and for some of them, the shifts become more prominent at the higher load. More importantly, more peaks show up in the frequency shift diagram (Fig. 2), i.e. more eigenmodes are affected. The increase in the vibration energy associated with the increase in the external load is re-distributed, affecting some of the existing modes to make the frequency shift more prominent and also triggering the frequency shift of other eigenmodes. The same characteristic is kept yet more significant when the load is further increased to 100 per cent gravity: not only a number of new eigenmodes are affected by the additional external work, but also the frequency shifts of quite a few existing peaks increase substantially.

Note that neither the change in the maximum frequency shift nor the occurrence frequency is linear to the magnitude of external loading, in part due to the non-linear shell theory used in the simulation. In addition, because the frequency shift does not occur continuously, the transported work done by the external loading associated with the vibration motion of the wing distributes non-uniformly over the frequency spectrum. The eigenmodes with large frequency shifts are those capable of being excited or suppressed relatively easily. Those for which the frequency shifts are negligible are of low-excitation/suppression factors.

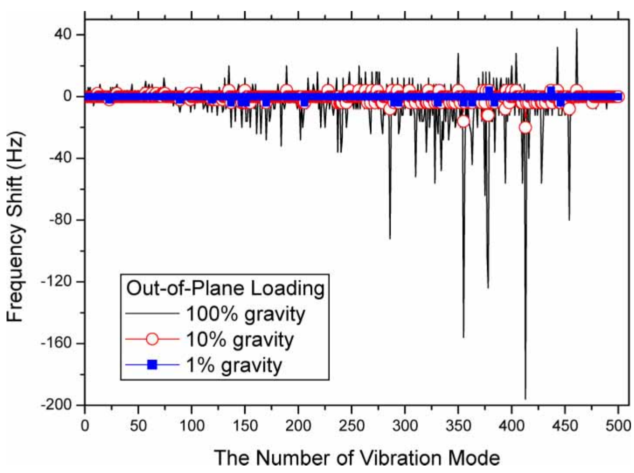

Fig. 2 Frequency shifts caused by out-of-plane loadings. The vibration modes are ranked by their corresponding natural vibration frequencies, with respect to 30 MHz. Altogether, 500 eigenmodes that are immediately above 30 MHz are studied

As the direction of the external load changes from out-of-plane to within the wing surface, both the number of affected eigenmodes and the magnitudes of corresponding frequency shifts vary. When the load is within the wing surface and normal to the axial direction, as shown in Fig. 3, the eigenmodes that are more sensitive to the transverse vibration are most affected. When the load is 1 per cent gravity, the magnitude of the maximum frequency shift, $\Delta\gamma$, is at the same level ($\sim$4 Hz), compared with the effects of the out-of-plane loading. As the load increases to 10 or 100 per cent gravity, it becomes evident that $\Delta\gamma$ is much smaller than their lateral (out-of-plane) loading counterparts. For instance, when the load is 100 per cent gravity, the maximum frequency shift is only $\sim$20 Hz, around one-tenth of that of the out-of-plane loading, which should be attributed to the fact that the moment of inertia of the wing is much larger along the transverse direction than that along the out-of-plane direction; thus, the vibration modes prefer to be excited normal to the wing surface for which the transverse load only has an indirect effect on these eigenmodes.

When the load is within the wing surface and along the axial direction, the pattern of the frequency shift, as shown in Fig. 4, is somewhat similar to that shown in Fig. 3, although the largest frequency shift occurs at different eigenmodes. This is because as the load is along the wave direction, the wing can be either 'stretched' or 'compressed', so that the vibrations are either promoted or suppressed, leading to an increase or decrease in the frequency, respectively. The overarching trend of frequency shift is similar to that shown in Fig. 3, i.e. most modes exhibit upshift during in-plane loading, whereas in Fig. 2, most modes exhibit downshift during out-of-plane loading. The phenomenon is analogous to the vibration of a deformed beam: when a beam is bent under out-of-plane loading (Fig. 2), its top surface is under tension, but the bottom surface is under compression. For the top surface, the frequency upshifts, whereas for the bottom surface, the frequency downshifts. Nevertheless, the downshift due to compression is always more prominent than the upshift due to tension, and thus more eigenmodes may have their frequencies downshifted. When an in-plane load is applied such that the beam (wing) is stretched (Figs 3 and 4), the frequencies prefer upshifting.

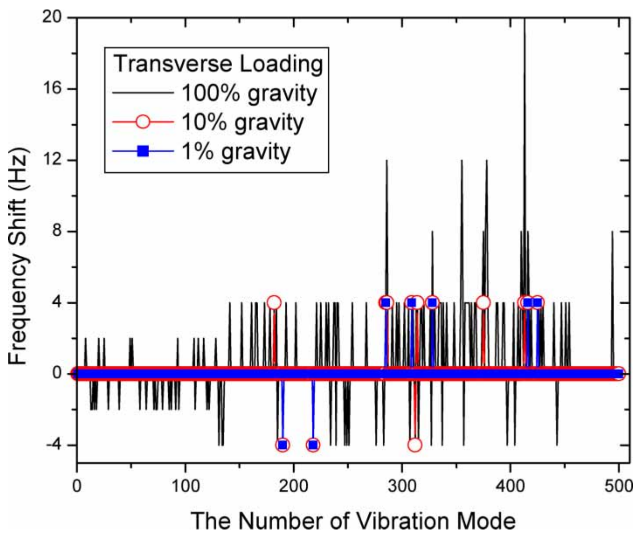

Fig. 3 Frequency shifts caused by transverse loadings

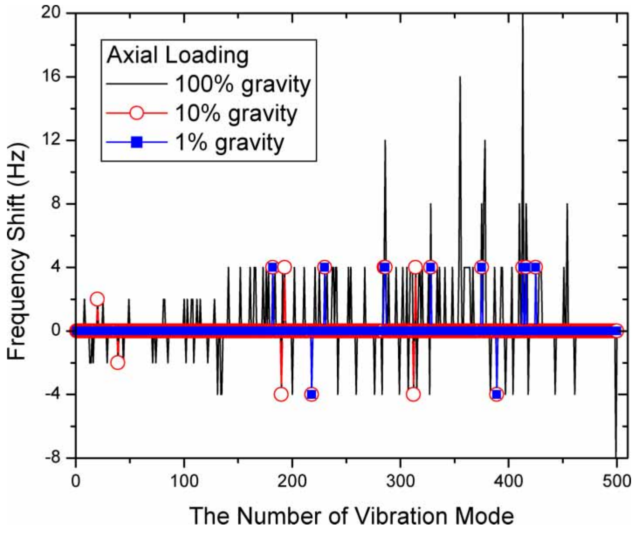

Fig. 4 Frequency shifts caused by axial loadings

Figure 5(a) shows the vibration amplitude of the 355th eigenmode when the wing vibrates freely, and Fig. 5(b) shows the difference in vibration amplitude as an external load (100 per cent gravity) normal to the wing surface is applied. Owing to the irregular shape of the wing and the fixed boundary condition, the largest amplitude occurs at the free end, and along the front–back direction, the vibration is asymmetric. At the leading edge, the amplitude is more close to the free end than that near the fixed end. At the trailing edge, the largest amplitude is reached in the mid-section and is slightly smaller than that at the front. The variation in the vibration amplitude follows a similar pattern. As the external load is applied, while more energy is provided, the amplitude tends to increase. The largest vibration amplitude happens at the free end and leading edge, and the magnitude change near the fixed end and trailing edge is negligible. Moreover, from the comparison between top and bottom surfaces, it is evident that the vibration amplitude at the bottom surface is larger than that at the top surface, with or without external loading, as the bottom surface is initially flat and therefore easier to vibrate. For the same reason, the difference in the vibration amplitude is more prominent at the bottom surface.

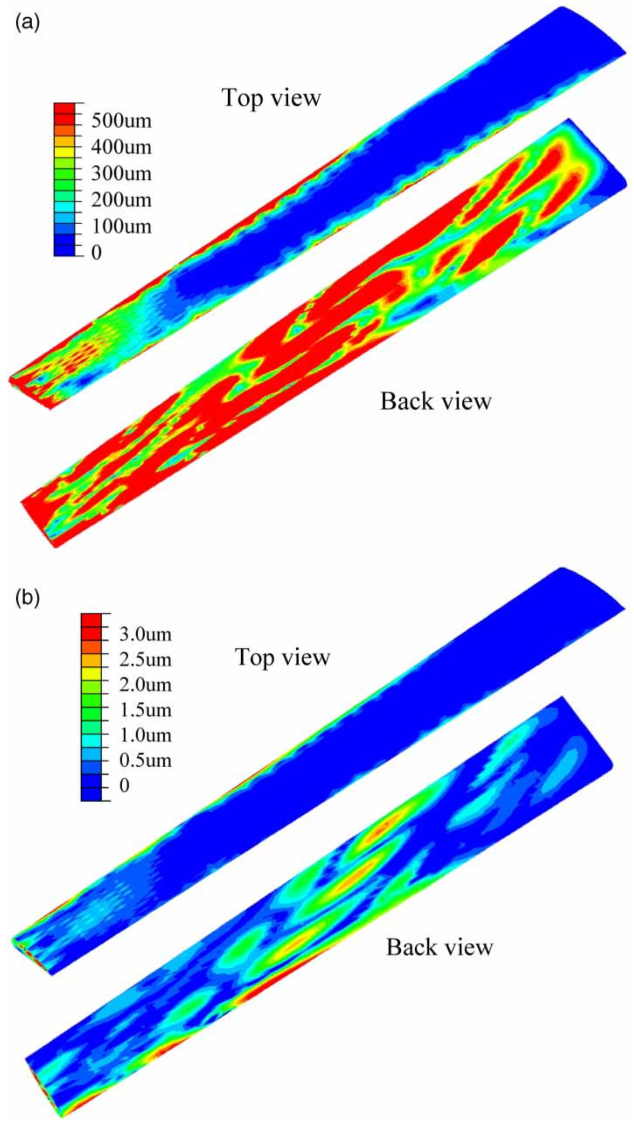

Fig. 5 Top and back views of the vibration amplitude at the 355th eigenmode: (a) without any external loading and (b) changes caused by the external loading

It is clear that the above discussion only provides a first-order approximation. A number of important issues, such as the coupling between the kinetic energy and the potential energy and the re-distribution of external work under various conditions, the influence of adjacent eigenmodes on both frequency shift and amplitude distribution, the effect of boundary condition, the spatial and temporal distributions of external loading, and airframe shape and compliance, demand more detailed study. In future, especially when a large-sized antenna or antenna arrays need to be placed along the vertical direction, other components of the airframe, such as tail wing or external support, must also be investigated. Nevertheless, the current simulation shows that there exists an evident coupling effect between the two main aspects of IAA: structural (load-carrying) and antenna (electromagnetic) properties. Moreover, the loading range is somewhat arbitrary. The lower end of the analysed load (10 per cent gravity) is more close to the actual situation, and the higher end ($\sim$100 per cent gravity) is discussed only for scientific analysis. It is shown that in all the cases, the variation in the high-frequency vibrational modes is significant, and this conclusion can be extended to broader loading ranges.

4 CONCLUDING REMARKS

In the current study, a proof-of-concept analysis of the frequency shift and the change in the magnitude of eigen vibration modes of an integrated antenna–wing structure for a small-sized unmanned aerial vehicle is performed. As an external load is induced by the antenna function, the high-frequency vibration modes of the wing are affected. The frequency shift does not take place uniformly over the frequency domain. The eigenmodes that can be easily excited are affected more pronouncedly than others. The largest frequency shift is caused by the out-of-plane loading. Depending on the nature of the eigenmode, the frequency may either increase or decrease. In the space domain, the variation in the vibration mode is also non-uniform. The largest change in the vibration amplitude takes place at the leading edge and at the free end of the wing.

ACKNOWLEDGEMENT

This work was supported by The National Science Foundation under Grants nos CMS-0623973 and CMS-0407743.

REFERENCES

1 **Drew, J. G.** *Unmanned aerial vehicle end to end support considerations*, 2006 (RAND Co., Cambridge, UK).
2 **Bone, E.** and **Bolkcom, C.** *Unmanned aerial vehicles: background and issues*, 2004 (Novinka Books, New York, NY).
3 **Anderson, J. D.** *Fundamentals of aerodynamics*, 2005 (McGraw-Hill, New York, NY).
4 **Balanis, C. A.** *Antenna theory: analysis and design*, 2005 (Wiley Inerscience, New York, NY).
5 **Balanis, C. A.** and **Ioannides, P.** The impact of smart antenna characteristics on network throughout and channel model BER: a review. *IEICE Trans. Elect.*, 2004, **E87C**, 1469–1476.
6 **Yu, K.** and **Ottersten, B.** Models for MIMO propagation channels: a review. *Wirel. Commun. Mobile Comput.*, 2002, **2**, 653–666.
7 **Winterhalter, C. A., Teverovsky, J., Wilson, P., Slade, J., Horowitz, W., Tierney, E.,** and **Sharma, V.** Development of

electronic textile to support networks, communications, and medical applications in future US military protective clothing systems. *IEEE Trans. Info. Tech. Biomed.*, 2005, **9**, 402–406.

8 **Yoon, K. J., Kim, Y. B., Kim, Y. S., Lee, J. D., Park, H. C., Goo, N. S.,** and **Lee, J. H.** Parametric study on compression deformation behavior of conformal load-bearing smart skin antenna structure. *Key Eng. Mater.*, 2004, **261–263**, 663–668.

9 **You, C. S.** and **Hwang, W. B.** Design of load-bearing antenna structures by embedding technology of microstrip antenna in composite sandwich structure. *Compos. Struct.*, 2005, **71**, 378–382.

10 **Schiek, B., Siweris, H. J.,** and **Rolfes, I.** *Noise in high-frequency circuits and oscillators*, 2006 (Wiley Interscience, New York, NY).

11 **Chou, Y. F.** and **Yang, M. Y.** Energy allocation in piezoelectric superlattices. In the ASME International Mechanical Engineering Congress and Exposition, Seattle, WA, 11–15 November 2007.

12 **Koo, J. H.** *Polymer nanocomposites*, 2006 (McGraw-Hill Prof., New York, NY).

13 **Ulaby, F. T.** *Fundamentals of applied electromagnetics*, 2006 (Prentice Hall, New York, NY).

14 **Thomson, W. T.** and **Dahleh, M. D.** *Theory of vibration with applications*, 1997 (Prentice Hall, New York, NY).